Transition State Theory Based Semi-Automatic Generation of Surface Reaction Mechanisms

P. Kraus, R. P. Lindstedt*

Department of Mechanical Engineering, Imperial College London, Exhibition Road, London SW7 2AZ, UK.

Abstract

The creation of reaction mechanisms suitable for microkinetic analysis of heterogeneous systems currently requires either experimentally derived sticking coefficients or major computational expense (e.g. ab initio, density functional or plane-wave methods). The present work focuses on developing a theoretical, reaction class based framework of estimating Arrhenius parameters in heterogeneous reaction systems. The framework is leveraging the unity bond index–quadratic exponential potential (UBI-QEP) method for estimating barrier heights, and combines an existing collision theory based method for estimation of homogeneous surface pre-exponential factors with the use of transition-state theory to replace experimental surface sticking coefficients in adsorption processes. Transition-state theory estimates for several reaction classes are produced in a semi-automated fashion, utilising the M06 family of density functionals and the Stuttgart-Dresden effective core potential for metal atoms. The present method is validated, analysed, and benchmarked against the sticking coefficient based method, for the case of partial ethane oxidation over a supported platinum catalyst. The the impact of key parameters (oxygen/carbon ratio, inlet velocity, site density and heat losses) is studied. Surface site fraction survey, and reaction pathway analysis is also performed, with a sensitivity study of the most important pathways included. The developed method reproduces experimental data with an accuracy comparable to the collision theory approach without the reliance on scarce, and sometimes conjectural, experimental parameters. The presented framework is well–suited for the efficient generation of heterogeneous reaction mechanisms for comparatively novel systems and can also serve to identify key pathways where the use of higher accuracy methods may be required.

Introduction

Most current computational frameworks for dealing with heterogeneous (surface) reactions use the extended 3-parameter Arrhenius form to describe reaction kinetics [1, 2, 3]. A number of frameworks for the estimation of the energy barrier has been formulated, such as the unity bond index–quadratic exponential potential (UBI-QEP) [4] method. On the other hand, estimation of adsorption pre-exponential factors within those frameworks relies on experimental sticking coefficients, the availability of which is a major issue in novel systems, with estimates also common in well-studied systems, especially for reactive species [5].

The present work focuses on developing a theoretical framework for estimating initial Arrhenius parameters for heterogeneous mechanisms, leveraging the UBI-QEP method for estimating barrier heights, and a reaction class-based method for estimation of pre-exponential factors, combining the widely used collision-theory for estimation of surface pre-exponential factors [1], and a simple transition-state theory approach to compute heterogeneous pre-exponentials.

Method

In the framework used by Vincent *et al.* [1], adsorption processes are treated using sticking coefficients. Bimolecular surface reactions are approximated by collisions based on 2-dimensional relative velocity, simulating the diffusion of the adsorbed species on the surface. Unimolecular reactions can not be treated using collision theory, therefore a very rudimentary transition-state estimate of $\frac{k_B T}{h}$ is used.

Sticking coefficients are generally derived from collision experiments in ultra high vacuum, where a known quantity of gas is admitted onto a clean surface. The sticking coefficient is then the ratio of the adsorbed over the admitted amount of gas [6]. The two classes of adsorption processes which require sticking coefficients have been modified to use a readily applied transition-state theory based approach. Additionally, desorption processes are treated more accurately and in a manner that is consistent with adsorption. The method for calculating pre-exponentials of homogeneous (surface) processes is unchanged from previous work [1], as the calculation method does not require experimental data. Table 1 presents an overview of the equations used to derive pre-exponentials in present work, compared to the widely used collision-theory approach.

Table 1: Comparison of formulas for determination of pre-exponential factors as AT^{β}. Partition functions highlighted in yellow and sticking coefficients in red.

Class	Present work	Collision theory [1]
Adsorption	$\frac{1}{x^x}\frac{k_B T}{h}\frac{Q_\ddagger}{Q_g}$	$\frac{s_0}{x^x} A_{Mt} N_A \Gamma \overline{v_{2D}}$
Eley-Rideal	$\frac{1}{x^x}\frac{k_B T}{h}\frac{Q_\ddagger}{Q_g}\frac{A_{B_s}}{A_{Mt}}$	$\frac{s_0}{x^x} A_{B_s} N_A \Gamma \overline{v_{2D}}$
Surface Bimolecular	$\frac{1}{3x^x}\frac{2b}{A_{Mt}}\overline{v_R}$	$\frac{1}{3x^x}\frac{2b}{A_{Mt}}\overline{v_R}$
Surface Unimolecular	$\frac{1}{x^x}\frac{k_B T}{h}$	$\frac{1}{x^x}\frac{k_B T}{h}$
Desorption	$\frac{k_B T}{h}\frac{Q_\ddagger}{Q_s}$	$\frac{k_B T}{h}$

Above, k_B, N_A and h are the Boltzmann, Avogadro and Planck constants, A_{Mt} and A_{B_s} are areas of the metal and the adsorbate B respectively, x is the number of additional empty platinum sites, T is the thermodynamic temperature, b is the collision radius of the colliding pair, and $\overline{v_R}$ and $\overline{v_{2D}}$ are the average relative and two-dimensional Maxwellian velocities, Γ is the site density of metal Mt.

The partition functions required in the equations above have been determined using standard formulas [6]:

- The translational contribution is obtained using classical methods.
- The electronic contribution is estimated as unity.
- The rotational contribution is based on moments of inertia from optimized structures obtained with Gaussian 09 [7].
- The vibrational contribution is calculated based on vibrational frequencies from the same structures.

For each species, the gas-phase, the adsorbed state, and a single

*Corresponding author: p.lindstedt@imperial.ac.uk

adsorption/desorption transition state partition function are required. Based on the principle of microscopic reversibility, the transition state of the adsorption process is the same as in the desorption process [6].

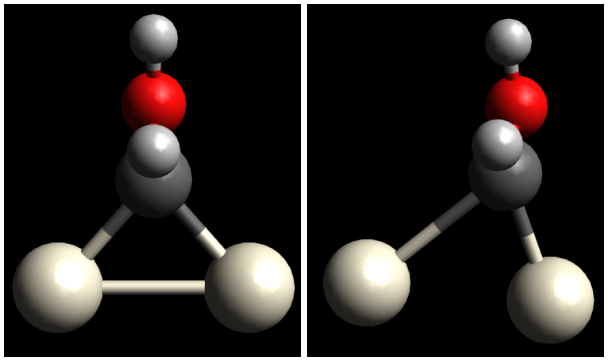

(a) (b)

Figure 1: Comparison of adsorbed state (a) and transition state (b) of CHOH on two Pt sites.

The gas-phase vibrational frequencies are determined using the M06-2X density functional [8] with the 6-31G(2df,p) basis set. Adsorbed and transition states are modelled using a simplified approach with the metal surface replaced by metal atoms (see Fig. 1). The M06 functional [8] was used, as the additional exchange in M06-2X made convergence difficult. A basis set of 6-311G(d,p) was used for C, O, H and the Stuttgart-Dresden effective core potential (SDD) [9] for the surface metal atoms.

The transition state was found by a relaxed potential energy surface (PES) scan starting from the adsorbed species, moving along the predicted direction of desorption using 0.1 Å spacing, with the metal atoms frozen. The position of the transition state was based on the shape of the PES, ensuring it has a single imaginary frequency acting along the direction of the breaking bond. Hindered rotors were treated automatically using the Pitzer–Gwinn method [10] as implemented in Gaussian 09 [7].

The surface treatment was chosen due to the favourable trade-off between accuracy and computational cost. While more advanced methods are available (e.g. cluster embedding), the current approach, coupled with UBI–QEP derived barrier heights, provides an effective way to build reaction mechanisms and to identify sensitive pathways that merit treatment using more accurate (and costly) *ab initio* or DFT methods.

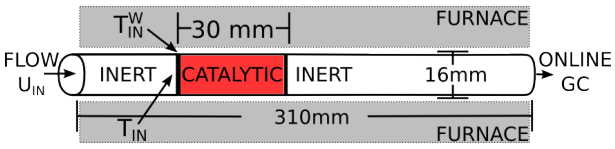

Figure 2: Overview of the reactor configuration.

Experimental Configuration

The case of partial catalytic oxidation of ethane over platinum (Pt) [1] was chosen for validation purposes. It is a complex system with active gas-phase and catalytic chemistries. Experimental data and simulations based on collision theory are also available. The experimental configuration follows that of Vincent *et al.* [1], schematically shown in Fig. 2. The catalytic section is 30 mm long, and contains 3 wt% Pt over α-Al_2O_3 support. Eight cases from the original study have been considered for this work, the conditions are listed in Table 2, and examine the effect of varying the O/C ratio (Cases 7, 9, 11, 12) and superficial inlet velocity (Cases 11, 12–16).

Table 2: Experimental conditions

Case	$\mathbf{L}_t$ [mm]	O/C	$\mathbf{U}_{in}$ [m/s]	$\mathbf{T}_{in}$ [K]	$\mathbf{T}^W_{in}$ [K]	$\mathbf{T}_{max}$ [K]
7	310	0.45	2.10	420	844	1318
9	310	0.55	2.10	421	890	1353
11	310	0.65	2.10	423	936	1386
12	310	0.70	2.10	424	981	1408
13	310	0.65	3.35	418	850	1338
14	310	0.65	4.18	408	806	1307
15	310	0.65	5.86	392	740	1263
16	310	0.65	6.72	383	681	1234

Computational Configuration

The computational methods are largely unchanged from previous work [1]. The same in-house FORTRAN 2D parabolic code [11] has been used, simulating a single, virtual, representative axi-symmetric pore. The pore radius has been estimated at $\sim$ 0.375 mm; the simulation contains 30 geometrically refined cells in the radial direction, corresponding to $\sim$ 2 µm resolution close to the catalytic surface. Initial axial steps are at 2 µm, with splitting applied if necessary. For reasons of consistency, the gas-phase chemistry is unchanged from previous work, despite updated gas-phase models being available [12], and features 44 species and 271 reactions [1].

Arrhenius parameters for the surface chemistry (A and T^β) have been updated based on Table 1, with the activation energies (E_A) retained from Vincent *et al.* [1]. The same surface mechanism has been used, comprising 35 surface species and 284 reversible reactions. Catalyst site density (Γ) and radiative heat loss factor (κ_2) have been retained at their median values of 7.5×10^{-8} kmol m^{-2} and 7% respectively [1].

Results and Discussion

Figure 3 shows the effect of varying O/C ratio. The conversion of both feedstocks is well represented at higher O/C ratios, slightly above the collision–theory data, both slightly overpredicting in the lowest case (O/C $= 0.45$). The present work improves agreement with experimental data in terms of the carbon selectivity. The oxygen selectivity deviates somewhat from the experimental data points, mainly due to the comparatively high CO_2 yield.

The effect of varying the inlet velocity is shown in Fig. 4. The conversion is consistent with experiment and collision theory, especially below velocities of 5 m s^{-1}. Similarly to the O/C ratio data, carbon selectivities are improved, and oxygen selectivities are in good agreement apart from the CO_2 data.

The overall agreement with the collision-theory derived mechanism is very good. The high CO_2 selectivity can be attributed to the oxygen adsorption rates, which are highly optimised in the collision theory model [1]. Similarly, CO is known to strongly adsorb on platinum and therefore the simplistic treatment of surface interaction in present work might not be sufficient. The over–prediction in conversion levels at low O/C and high velocities is shared with the collision theory data.

A sensitivity study of the impact of the catalyst site density (Γ) has been carried out. Values larger than the default 7.5×10^{-8} kmol m^{-2} had no effect on simulation results. Smaller

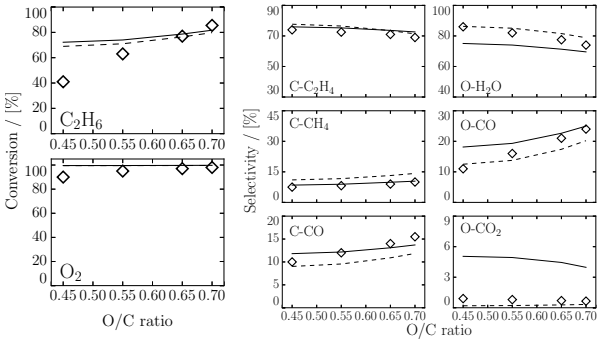

Figure 3: Effect of varying O/C ratio on (left) ethane and oxygen conversion, (right) selectivity to major species. Diamonds ($\diamond$) represent experimental data, dashed line ($--$) represents collision-theory results, full line (—) corresponds to present work data.

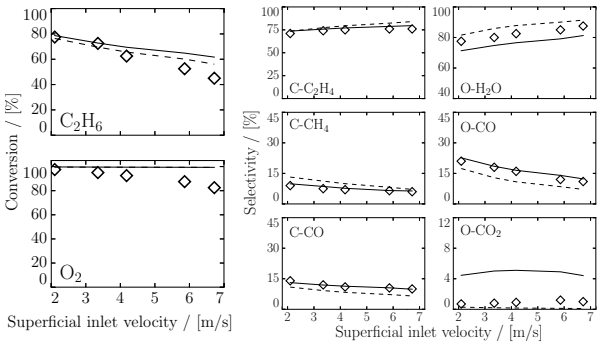

Figure 4: Effect of varying inlet velocity on (left) ethane and oxygen conversion, (right) selectivity to major species.

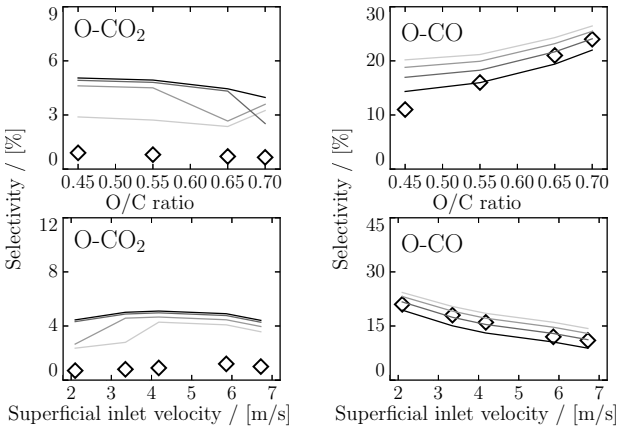

Figure 5: Effect on oxygen selectivity to CO_2 for $\Gamma = 5.0, 6.0, 7.0$ and 7.5×10^{-8} kmol m^{-2} (left). Effect on oxygen selectivity to CO for $\kappa_2 = 0, 5, 10$ and 15% (right).

values mainly affect the oxygen selectivity to CO_2 (Fig. 5) and, to lesser extent, the carbon selectivity to CH_4. The impact of the radiative heat loss factor (κ_2) has also been examined for the range between 0 and 15%. The most profound effect can be found in the oxygen selectivity to CO (Fig. 5).

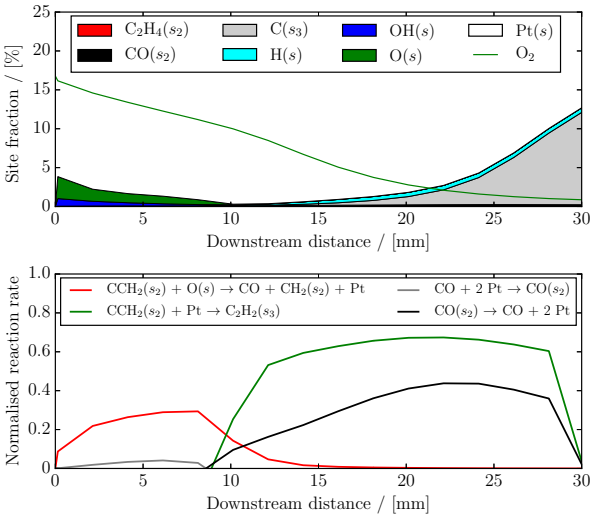

Figure 6: Site fractions of major species for Case 11. Green line denotes molar fraction of O_2 near the surface (top). Key reaction rates in CO and C(s_3) formation (below).

Surface site fraction analysis of Case 11 (Fig. 6) shows that more than 80% of catalytic sites remain unoccupied at all times. Initially, oxygen is adsorbed on the surface, but between 10 and 15 mm downstream, carbon deposition starts taking place. This change in catalytic activity can not be attributed to oxygen depletion in the gas phase, as at that point the O_2 mol fraction is approximately 10 mol$\%$ (green line in top graph of Fig. 6). A pathway analysis shows an initial dominance of ethane adsorption followed by dehydrogenation:

$$\begin{aligned} C_2H_6 + 2\,Pt &\rightarrow C_2H_6(s_2) && (1)\\ C_2H_6(s_2) + O(s) &\rightarrow C_2H_5(s) + OH(s) && (119)\\ C_2H_5(s) + Pt &\rightarrow C_2H_4(s) + H(s) && (150) \end{aligned}$$

accompanied with production of CO_2. This is a two step process involving (1) adsorption of CO produced from $CCH_2(s_2)$ via (251) and (378) (also see Fig. 6)

$$\begin{aligned} CCH_2(s_2) + O(s) &\rightarrow CO + CH_2(s_2) && (251)\\ CO + 2\,Pt &\rightarrow CO(s_2) && (378) \end{aligned}$$

and (2) surface oxidation of CHO(s) and $CO(s_2)$ to $CO_2(s)$ via reactions (461), (389) and (475).

$$\begin{aligned} CHO(s) + 2\,Pt &\rightarrow CO(s_2) + H(s) && (461)\\ CO(s_2) + OH(s) &\rightarrow COOH(s) + 2\,Pt && (389)\\ COOH(s) + 2\,Pt &\rightarrow CO_2(s) + H(s) && (475) \end{aligned}$$

Consistent with the surface site fraction analysis, around the 10 mm mark, desorption of CO becomes more favourable than its adsorption, leading to production of $C_2H_2(s_3)$ from $CCH_2(s_2)$ (green line in Fig. 6) and further decomposition:

$$\begin{aligned} CCH_2(s_2) + Pt &\rightarrow C_2H_2(s_3) && (274)\\ C_2H_2(s_3)+H_2+Pt &\rightarrow CHCH_2(s_3)+H(s) && (232)\\ CHCH_2(s_3) &\rightarrow CHCH_2(s) + 2\,Pt && (215)\\ CHCH_2(s) + 3\,Pt &\rightarrow C_2H_2(s_3) + H(s) && (207) \end{aligned}$$

The above hydrogenation/isomerisation chain is fast. However, both isomers of $CHCH_2$ can further decompose:

$$\begin{aligned} \mathrm{CHCH_2}(s_3) + \mathrm{Pt} &\rightarrow \mathrm{C}(s_3) + \mathrm{CH_3}(s) \quad (221)\\ \mathrm{CHCH_2}(s) + 3\,\mathrm{Pt} &\rightarrow \mathrm{C}(s_3) + \mathrm{CH_3}(s) \quad (197)\\ \mathrm{CH_3}(s) + \mathrm{H}(s) &\rightarrow \mathrm{CH_4} + 2\,\mathrm{Pt} \quad (303) \end{aligned}$$

Reactions (221) and (197) are the main methyl producing channels in the latter stages of the process. Methane, upon formation, does not tend to readsorb, effectively forming a sink. Finally, carbon deposited on the surface as $\mathrm{C}(s_3)$ does not react further, apart from catalysing $\mathrm{H_2}$ adsorption in:

$$\begin{aligned} \mathrm{H_2} + \mathrm{C}(s_3) + \mathrm{Pt} &\rightarrow \mathrm{CH}(s_3) + \mathrm{H}(s) \quad (350)\\ \mathrm{CH}(s_3) + \mathrm{Pt} &\rightarrow \mathrm{C}(s_3) + \mathrm{H}(s) \quad (360) \end{aligned}$$

Conclusion

In present work, a revised framework for generation of surface reaction mechanisms has been proposed and validated for the case of partial catalytic oxidation of ethane over platinum. The current transition–state theory based approach provides good agreement with experimental data and, when compared to a previous collision theory model [1], similar selectivity and conversion characteristics as shown in Figs. 3 and 4. A pathway analysis explains the decrease in CO production (Fig. 6) when higher heat losses are imposed, the decrease of production of CH_4 and CO at higher velocities (Fig. 4) due to blow-off and lower temperatures. The pathway leading to the experimentally observed carbon deposition (as $\mathrm{C}(s_3)$) is also explained.

The results obtained are encouraging and the current approach is currently under investigation in order to provide further validation for different experimental datasets, with varying geometries and conditions, on the $\mathrm{C_2H_6/O_2/Pt}$ system, and also on simpler systems, such as $\mathrm{H_2/O_2/Pt}$ and $\mathrm{CH_4/O_2/Pt}$.

Acknowledgements

We wish to express our gratitude for the assistance and continued encouragement of Dr. I. A. B. Reid. We would also like to thank Dr I. Sakata and Dr K. Gkagkas of Toyota Motor Europe for supporting the development of this framework for use in internal combustion engine related applications.

References

[1] Vincent, R. S. *et al.*, J. Cat. 260 (2008) 37.
[2] Kee, R. J. *et al.*, Chemkin Collection, 3rd Edition, Reaction Design Inc. (2000).
[3] Deutschmann, O. *et al.*, DETCHEM Software Package, 2nd Edition, Karlsruhe (2012).
[4] Shustorovich, E. and Sellers, H., Surf. Sci. Rep. 31 (1998) 1.
[5] Zerkle, D. *et al.*, J. Cat. 196 (2000) 18.
[6] Dumesic, J. A. *et al.*, The microkinetics of heterogeneous catalysis, ACS (1993).
[7] Frisch, M. J. *et al.*, Gaussian 09 Revision D.01, Gaussian Inc. (2009).
[8] Zhao, Y. and Truhlar, D. G., Theor. Chem. Acc. 120 (2008) 215-241.
[9] Andrae, D. *et al.*, Theor. Chem. Acc. 77 (1990).
[10] Pitzer, K. S. and Gwinn, W. D., J. Chem. Phys. 10 (1942) 428-440.
[11] Leung, K. M. and Lindstedt, R. P., Combust. Flame 102 (1995) 129-160.
[12] Robinson, R. K. and Lindstedt, R. P., Comb. Flame 160 (2013) 2642-2653.

Table Of Selected Reaction Rates

#	Reaction	A	β	E_A
(1)	C2H6 + 2 PTW = C2H6W2	1.5727E+07	0.5	0.0
(2)	C2H6W2 = C2H6 + 2 PTW	4.4757E+11	1.0	36.1
(119)	C2H6W2 + OW = OHW + CH2CH3W + PTW	1.5523E+11	0.5	7.9
(120)	OHW + CH2CH3W + PTW = C2H6W2 + OW	1.6856E+11	0.5	34.6
(149)	HW + C2H4W = CH2CH3W + PTW	4.8023E+11	0.5	22.7
(150)	CH2CH3W + PTW = HW + C2H4W	9.9827E+10	0.5	26.4
(197)	CHCH2W + 3 PTW = CW3 + CH3W	3.8303E+09	0.5	42.0
(198)	CW3 + CH3W = CHCH2W + 3 PTW	1.7693E+11	0.5	84.9
(207)	CHCH2W + 3 PTW = C2H2W3 + HW	3.8303E+09	0.5	19.0
(208)	C2H2W3 + HW = CHCH2W + 3 PTW	4.9669E+11	0.5	73.6
(215)	CHCH2W3 = CCH3W3	2.0837E+10	1.0	21.0
(216)	CCH3W3 = CHCH2W3	2.0837E+10	1.0	78.0
(221)	CHCH2W3 + HW = C2H2 + H2W + 3 PTW	4.5614E+11	0.5	71.6
(222)	C2H2 + H2W + 3 PTW = CHCH2W3 + HW	3.2301E+06	1.0	0.0
(231)	CCH3W3 + PTW = CW3 + CH3W	9.8722E+10	0.5	46.3
(232)	CW3 + CH3W = CCH3W3 + PTW	1.7693E+11	0.5	83.2
(251)	CCH2W2 + OW = CH2O + CW3	1.5359E+11	0.5	44.2
(252)	CH2O + CW3 = CCH2W2 + OW	8.6783E+05	0.5	71.6
(273)	C2H2W3 = C2H2 + 3 PTW	2.2271E+10	1.0	134.0
(274)	C2H2 + 3 PTW = C2H2W3	3.7052E+06	1.0	0.0
(303)	CH3W + HW + PTW = CH2W2 + H2W	4.0967E+11	0.5	137.7
(304)	CH2W2 + H2W = CH3W + HW + PTW	3.2225E+11	0.5	5.9
(349)	CHW3 + OW = CHO + 4 PTW	1.5829E+11	0.5	45.6
(350)	CHO + 4 PTW = CHW3 + OW	5.4062E-01	0.0	45.0
(359)	CW3 + OW = CO + 4 PTW	1.4814E+11	0.5	53.9
(360)	CO + 4 PTW = CW3 + OW	2.6177E-01	0.5	92.6
(377)	COW2 + OW = CO2W2 + PTW	1.4122E+11	0.5	97.4
(378)	CO2W2 + PTW = COW2 + OW	7.9579E+10	0.5	154.2
(389)	COW2 + H2W + PTW = COHW3 + HW	3.2125E+11	0.5	127.8
(390)	COHW3 + HW = COW2 + H2W + PTW	4.3957E+11	0.5	29.0
(461)	CHOW + HW = CO + H2W + PTW	4.3438E+11	0.5	35.1
(462)	CO + H2W + PTW = CHOW + HW	7.1853E+02	1.0	0.0
(475)	COOHW + HW + PTW = COW2 + H2OW	4.6545E+11	0.5	28.6
(476)	COW2 + H2OW = COOHW + HW + PTW	1.5258E+11	0.5	86.6

Data above to be used with the extended Arrhenius formula: $k = \mathrm{AT^{\beta}e^{\frac{-E_A}{RT}}}$, A in $\mathrm{s^{-1}}$, and E_A in kJ $\mathrm{mol^{-1}}$. The reaction rate constants k are presented as $\mathbb{R} = \frac{k}{\Gamma^{m-1}} \prod [X_i]$, where m is the total number of Pt sites involved in the reaction and Γ is the site density.